

META-DYNAMICAL STATE SPACE MODELS FOR INTEGRATIVE NEURAL DATA ANALYSIS

Ayesha Vermani¹, Josue Nassar², Hyungju Jeon¹, Matthew Dowling¹, Il Memming Park¹

¹ Champalimaud Centre for the Unknown, Champalimaud Foundation, Portugal

² RyvivyR, USA

{ayesha.vermani, memming.park}@research.fchampalimaud.org

ABSTRACT

Learning shared structure across environments facilitates rapid learning and adaptive behavior in neural systems. This has been widely demonstrated and applied in machine learning to train models that are capable of generalizing to novel settings. However, there has been limited work exploiting the shared structure in neural activity during similar tasks for learning latent dynamics from neural recordings. Existing approaches are designed to infer dynamics from a single dataset and cannot be readily adapted to account for statistical heterogeneities across recordings. In this work, we hypothesize that similar tasks admit a corresponding family of related solutions and propose a novel approach for meta-learning this solution space from task-related neural activity of trained animals. Specifically, we capture the variabilities across recordings on a low-dimensional manifold which concisely parametrizes this family of dynamics, thereby facilitating rapid learning of latent dynamics given new recordings. We demonstrate the efficacy of our approach on few-shot reconstruction and forecasting of synthetic dynamical systems, and neural recordings from the motor cortex during different arm reaching tasks.

1 INTRODUCTION

Latent variable models are widely used in neuroscience to extract dynamical structure underlying high-dimensional neural activity (Pandarinath et al., 2018; Schimel et al., 2022; Dowling et al., 2024). While latent dynamics provide valuable insights into behavior and generate testable hypotheses of neural computation (Luo et al., 2023; Nair et al., 2023), they are typically inferred from a single recording session. As a result, these models are sensitive to small variations in the underlying dynamics and exhibit limited generalization capabilities. In parallel, a large body of work in machine learning has focused on training models from diverse datasets that can rapidly adapt to novel settings. However, there has been limited work on inferring generalizable dynamical systems from data, with existing approaches mainly applied to settings with known low-dimensional dynamics (Yin et al., 2021; Kirchmeyer et al., 2022).

Integrating noisy neural recordings from different animals and/or tasks for learning the underlying dynamics presents a unique set of challenges. This is partly due to heterogeneities in recordings across sessions such as the number and tuning properties of recorded neurons, as well as different stimulus statistics and behavioral modalities across cognitive tasks. This challenge is further compounded by the lack of inductive biases for disentangling the variabilities across dynamics into shared and dataset-specific components. Recent evidence suggests that learned latent dynamics underlying activity of task-trained biological and artificial neural networks demonstrate similarities when engaged in related tasks (Gallego et al., 2018; Maheswaranathan et al., 2019; Safaie et al., 2023). In a related line of work, neural networks trained to perform multiple cognitive tasks with overlapping cognitive components learn to reuse dynamical motifs, thereby facilitating few-shot adaptation on novel tasks (Turner & Barak, 2023; Driscoll et al., 2024).

Motivated by these observations, we propose a novel framework for meta-learning latent dynamics from neural recordings. Our approach is to encode the variations in the latent dynamical structure present across neural recordings in a low-dimensional vector, $e \in \mathbb{R}^{d_e}$, which we refer to as the *dynamical embedding*. During training, the model learns to adapt a common latent dynamical system

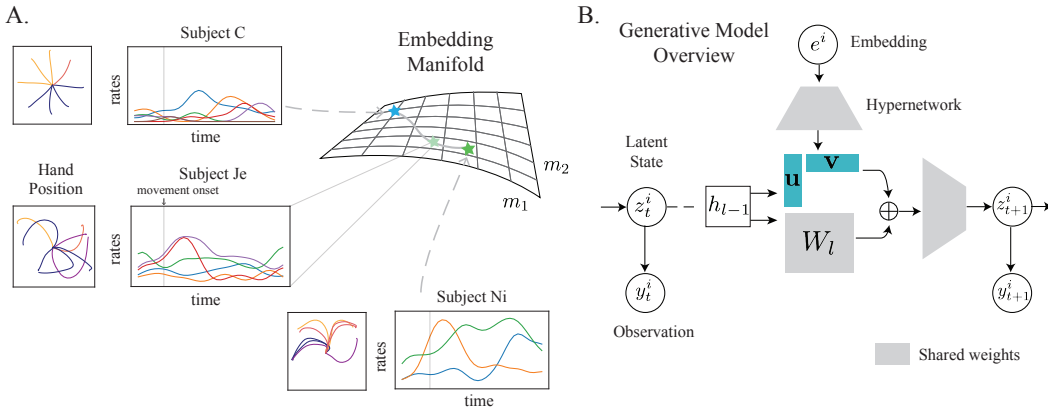


Figure 1: **A.** Neural recordings display heterogeneities in the number and tuning properties of recorded neurons and reflect diverse behavioral responses. The low-dimensional embedding manifold captures this diversity in dynamics. **B.** Our method learns to adapt a common latent dynamics conditioned on the embedding via low-rank changes to the model parameters.

model conditioned on the dynamical embedding. We learn the dynamical embedding manifold from a diverse collection of neural recordings, allowing rapid learning of latent dynamics in the analysis of data-limited regime commonly encountered in neuroscience experiments.

Our contributions can be summarized as follows:

1. We propose a novel parameterization of latent dynamics that facilitates integration and learning of meta-structure over diverse neural recordings.
2. We develop an inference scheme to jointly infer the embedding and latent state trajectory, as well as the corresponding dynamics model directly from data.
3. We demonstrate the efficacy of our method on few-shot reconstruction and forecasting for synthetic datasets and motor cortex recordings obtained during different reaching tasks.

2 CHALLENGES WITH JOINTLY LEARNING DYNAMICS ACROSS DATASETS

Neurons from different sessions and/or subjects are partially observed, non-overlapping and exhibit diverse response properties. Even chronic recordings from a single subject exhibit drift in neural tuning over time (Driscoll et al., 2022). Moreover, non-simultaneously recorded neural activity lack pairwise correspondence between single trials. This makes joint inference of latent states and learning the corresponding latent dynamics by integrating different recordings ill-posed and highly non-trivial.

As an illustrative example, let’s consider a case where these recordings exhibit oscillatory latent dynamics with variable velocities (Fig. 2A). One possible strategy for jointly inferring the dynamics from these recordings is learning a shared dynamics model, along with dataset-specific likelihood functions that map these dynamics to individual recordings. However, without additional inductive biases, this strategy does not generally perform well when there are variabilities in the underlying dynamics. Specifically, when learning dynamics from two example datasets ($M = 2$), we observed that a model with shared dynamics

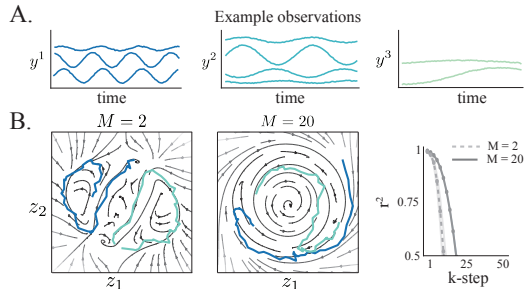


Figure 2: **A.** Three different example neural recordings, where the speed of the latent dynamics varies across them. **B.** One generative model is trained on $M = 2$ and $M = 20$ datasets. While increasing the number of datasets allows the model to learn limit cycle, it is unable to capture the different speeds leading to poor forecasting performance.

either learned separate solutions or overfit to one dataset, obscuring global structure across recordings (Fig. 2A). When we increased the diversity of training data ($M = 20$), the dynamics exhibited a more coherent global structure, albeit with an overlapping solution space (Fig. 2B). As a result, this model had poor forecasting performance of neural activity in both cases, which is evident in the k-step r^2 (Fig. 2B). While we have a-priori knowledge of the source of variations in dynamics for this example, this is typically not the case with real neural recordings. Therefore, we develop an approach for inferring the variation across recordings and use it to define a solution space of related dynamical systems (Fig. 1A).

3 INTEGRATING NEURAL RECORDINGS FOR META-LEARNING DYNAMICS

Let $y_{1:T}^{1:M}$ denote neural time series datasets of length T , with $y_t^i \in \mathbb{R}^{d_y^i}$, collected from M different sessions and/or subjects during related tasks. We are interested in learning a generative model that can jointly describe the evolution of the latent states across these datasets and rapidly adapt to novel datasets from limited trajectories. In this work, we focus on state-space models (SSM), a powerful class of generative models for spatio-temporal datasets. An SSM is described via the following pair of equations (we drop the superscript for ease of presentation),

$$z_t | z_{t-1} \sim p_\theta(z_t | z_{t-1}), \quad (1)$$

$$y_t | z_t \sim p_\phi(y_t | z_t), \quad (2)$$

where $z_t \in \mathbb{R}^{d_z}$ is the latent state at time t , $p_\theta(z_t | z_{t-1})$ is the dynamics model and $p_\phi(y_t | z_t)$ is the likelihood function that maps the latent state to observed data.

Following standard practice, we parameterize the dynamics as $p_\theta(z_t | z_{t-1}) = \mathcal{N}(z_t | f_\theta(z_{t-1}), Q)$, where f_θ is a deep neural network (DNN) and Q is a covariance matrix¹. As previous work has shown that making both the likelihood and dynamics highly expressive can lead to optimization issues (Bowman et al., 2015), we model the likelihood as a linear function of z_t . For instance; for real-valued observations, it is defined as $p_\phi(y_t | z_t) = \mathcal{N}(y_t | Cz_t + D, R)$.

3.1 HIERARCHICAL STATE-SPACE MODEL FOR MULTIPLE DATASETS

To learn an SSM that can jointly describe the spatio-temporal evolution across M neural recordings, we introduce a hierarchical structure in the latent dynamics model that captures the variations in dynamics across datasets. A natural choice for learning such a generative model is a fully Bayesian approach, where each dataset would have its own latent dynamics, parameterized by θ^i , and a hierarchical prior would be used to tie the dataset specific parameters to the shared parameters, $\theta \sim p(\theta)$ (Linderman et al., 2019), leading to the following generative model

$$\theta^i | \theta \sim p(\theta^i | \theta), \quad (3)$$

$$z_t^i | z_{t-1}^i, \theta^i \sim \mathcal{N}(z_t^i | f_{\theta^i}(z_{t-1}^i), Q^i), \quad (4)$$

$$y_t^i | z_t^i \sim p_{\phi^i}(y_t^i | z_t^i), \quad (5)$$

where dataset specific likelihoods, $p_{\phi^i}(y_t^i | z_t^i)$, are used to account for different dimensionality and/or modality of recordings.

If we assume that $p(\theta^i | \theta)$ is Gaussian, i.e., $p(\theta^i | \theta) = \mathcal{N}(\theta^i | \theta, \Sigma)$, we can equivalently express dynamics for the hierarchical generative model as,

$$\varepsilon^i \sim \mathcal{N}(\varepsilon^i | 0, \Sigma), \quad (6)$$

$$z_t^i | z_{t-1}^i, \theta, \varepsilon^i \sim \mathcal{N}(z_t^i | f_{\theta+\varepsilon^i}(z_{t-1}^i), Q^i), \quad (7)$$

where the dataset-specific dynamics parameter, θ^i , is expressed as a sum of the shared parameters, θ , and a dataset-specific term, ε^i . This decomposition of latent dynamics explicitly introduces an inductive bias that encourages θ and ε^i to capture the shared and dataset-specific dynamical structure respectively. While this formulation is appealing, the equal dimensionality of ε^i and θ could lead the model to overly rely on dataset-specific terms. Additionally, using DNNs for modeling latent dynamics introduces a large number of parameters, thereby limiting the scalability of this approach.

¹We note that Q can also be parameterized via a neural network as well.

Drawing inspiration from the hierarchical Bayesian model, we develop an alternative hierarchical framework that both improves scalability and more effectively incorporates the desired inductive bias. Specifically, we introduce a low-dimensional latent variable, $e^i \in \mathbb{R}^{d_e}, \mathbb{R}^{d_e} \ll \mathbb{R}^{d_\varepsilon}$ —which we refer to as the dynamical embedding—that maps to the space of dynamics parameters and encodes dataset-specific variations (Rusu et al., 2019). This approach enhances scalability and enables efficient few-shot learning, as it requires simply inferring the embedding given new data.

The generative model for this hierarchical SSM is then described as,

$$e^i \sim p(e), \quad (8)$$

$$z_t^i | z_{t-1}^i, e^i \sim \mathcal{N}(z_t^i | f_\theta(z_{t-1}^i, e^i), Q^i), \quad (9)$$

$$y_t^i | z_t^i \sim p_{\phi^i}(y_t^i | z_t^i), \quad (10)$$

where we drop the prior over the shared dynamics parameter, θ , significantly reducing the dimensionality of the inference problem. Similar to the hierarchical Bayesian model, all datasets share the same latent dynamics, θ , with the dataset-specific variation captured by the dynamical embedding, e_i .

Next, we expand on the functional form of the latent dynamics f_θ conditioned on e^i . Our goal is to design f_θ in a way that can effectively capture complex changes and disentangle underlying variability in dynamics across recordings, while simultaneously incentivizing the extraction of shared dynamical structure. While the simplest formulation would be using the embedding as an input to the dynamics model (Zintgraf et al., 2019; Cotler et al., 2023), we observed that this led to interference between dynamics as we increased the diversity of dynamical regimes (for example, Fig. 13). Instead, we use the dynamical embeddings to directly output changes to the parameters of the dynamics model via a hypernetwork, h_ϑ , (Ha et al., 2016), which facilitates increased expressivity when modeling conditional functions (Galanti & Wolf, 2020),

$$\theta^i = \theta + h_\vartheta(e^i), \quad (11)$$

$$z_t^i | z_{t-1}^i, e^i \sim \mathcal{N}(z_t^i | f_{\theta^i}(z_{t-1}^i), Q^i). \quad (12)$$

We encourage learning of shared dynamical structure by constraining h_ϑ to make low-rank changes to the parameters of f_θ (Fig. 1B). For example, if we parameterize f_θ as a 2-layer fully-connected network and constrain the hypernetwork to only make rank $d^r = r$ changes to the hidden weights, then f_{θ^i} would be expressed as,

$$f_{\theta^i}(z_t^i) = \mathbf{W}_o \sigma(\underbrace{\{\mathbf{W}_{hh} + h_\vartheta(e^i)\}}_{\text{embedding modification}} \sigma(\mathbf{W}_{in} z_t^i)) \quad (13)$$

$$= \underbrace{\mathbf{W}_o}_{\mathbb{R}^{d_z \times d_2}} \sigma(\underbrace{\{\mathbf{W}_{hh}\}}_{\mathbb{R}^{d_2 \times d_1}} + \underbrace{\mathbf{u}_\vartheta(e^i)}_{\mathbb{R}^{d_2 \times d_r}} \cdot \underbrace{\mathbf{v}_\vartheta(e^i)^\top}_{\mathbb{R}^{d_r \times d_1}}) \sigma(\underbrace{\mathbf{W}_{in}}_{\mathbb{R}^{d_1 \times d_z}} z_t^i) \quad (14)$$

where $\sigma(\cdot)$ denotes a point-nonlinearity, and the two functions $\mathbf{v}_\vartheta(e^i) : \mathbb{R}_e^d \rightarrow \mathbb{R}^{d_1 \times r}$, $\mathbf{u}_\vartheta(e^i) : \mathbb{R}_e^d \rightarrow \mathbb{R}^{d_2 \times r}$ map the embedding representation to form the low-rank perturbations, and both \mathbf{u}_ϑ and \mathbf{v}_ϑ are parameterized by a neural network.

3.2 INFERENCE AND LEARNING

Given $y_{1:T}^{1:M}$, we want to infer both the latent states, $z_{1:T}^{1:M}$ and the dynamical embeddings, $e^{1:M} = [e^1, \dots, e^M]$ as well as learn the parameters of the generative model, $\Theta = \{\theta, \vartheta, \phi^1, \dots, \phi^M\}$. Exact inference and learning requires computing the posterior, $p_\Theta(z_{1:T}^{1:M}, e^{1:M} | y_{1:T}^{1:M})$, and log marginal likelihood, $\log p_\Theta(y_{1:T}^{1:M})$, which are both intractable. To circumvent this issue, we use a sequential variational autoencoder (seqVAE) (Krishnan et al., 2015)—an extension of variational autoencoders for state-space models—to learn the generative model by optimizing a lower-bound to the log marginal likelihood (commonly referred to as the ELBO). The ELBO for $y_{1:T}^{1:M}$ is defined as,

$$\begin{aligned} \mathcal{L}(y_{1:T}^{1:M}) = & \sum_{t,m} \mathbb{E}_{q_{\alpha,\beta}} [\log p_{\phi^i}(y_t^i | z_t^i)] \\ & - \mathbb{E}_{q_\beta} [\mathbb{D}_{KL}(q_\beta(z_t^i | \bar{y}_{1:T}^i, e^i) || p_{\theta,\vartheta}(z_t^i | z_{t-1}^i, e^i))] - \mathbb{D}_{KL}(q_\alpha(e^i | \bar{y}_{1:T}^i) || p(e^i)) \end{aligned} \quad (15)$$

where $q_\alpha(e^i | \bar{y}_{1:T}^i)$ and $q_\beta(z_t | \bar{y}_{1:T}^i, e^i)$ are the encoders for the dynamical embedding and latent state, respectively, and $\mathbb{E}_{q_{\alpha,\beta}} \equiv \mathbb{E}_{q_\beta(z_t | \bar{y}_{1:T}^i, e^i) q_\alpha(e^i | \bar{y}_{1:T}^i)}$. We additionally train a per-dataset read-in

network $\Omega_i : \mathbb{R}^{d_y^i} \rightarrow \mathbb{R}^{d_{\bar{y}}}$ that maps y_t^i to a vector $\bar{y}_t^i \in \mathbb{R}^{d_{\bar{y}}}$. As described in Sec. 2, one of the challenges with integrating recordings in a common latent space is different dimensionalities (number of recorded neurons) and the dependence of neural activity on the shared latent space. The read-in network ensures that the latent states and dynamical-embeddings inferred from each dataset live in the same space.

We use the following parametrization of the inference networks (Krishnan et al., 2015),

$$\bar{y}_t^i = \Omega^i(y_t^i), \tag{16}$$

$$q_\alpha(e^i | \bar{y}_{1:T}^i) = \mathcal{N}(e^i | \mu_\alpha(\bar{y}_t^i), \sigma_\alpha^2(\bar{y}_t^i)), \tag{17}$$

$$q_\beta(z_{1:T}^i | \bar{y}_{1:T}^i, e^i) = \prod_{t=1}^T \mathcal{N}(z_t^i | \mu_\beta(\text{concat}(\bar{y}_t^i, e^i)), \sigma_\beta^2(\text{concat}(\bar{y}_t^i, e^i))), \tag{18}$$

where concat is the concatenation operation. We parameterize $\mu_\alpha, \sigma_\alpha^2$ by a bidirectional recurrent neural network, and $\mu_\beta, \sigma_\beta^2$ by a regular recurrent network. We emphasize that $\mu_\alpha, \sigma_\alpha^2, \mu_\beta,$ and σ_β^2 are shared across all datasets.

3.3 PROOF OF CONCEPT

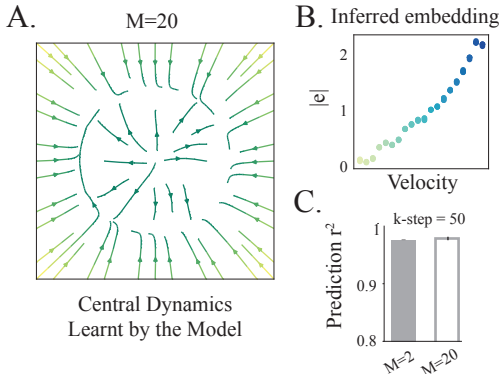


Figure 3: **A.** Example dynamics learned by the proposed approach when trained with $M = 20$ datasets. **B.** Samples from the inferred dynamical embedding for each dataset (see eq. 17). **C.** Forecasting r^2 at k-step=50 for models trained with $M = 2$ and $M = 20$ datasets.

As a proof of concept, we revisit the motivating example presented in Section 2 as a means to validate the efficacy of our approach and investigate how it unifies dynamics across datasets. For both $M = 2$ and $M = 20$ datasets, we used an embedding dimensionality of 1 and allowed the network to make a rank-1 change to the dynamics parameters.

After training, we observed that the shared dynamics (when $e = 0$) converged to a limit cycle with a slow velocity (Fig. 3A)—capturing the global topology that is shared across all datasets—and the model learned to modulate the velocity of the dynamics conditioned on the dynamical embedding which strongly correlated with the dataset specific velocity² (Fig 3B). This demonstrated that the proposed approach is able to capture dataset-specific variability. Lastly, Fig. 3C demonstrates that the proposed approach is able to forecast well for both $M = 2$ and $M = 20$ datasets. We include further validation experiments when there is no model mismatch

as well as the generalization of the trained model to new data in Appendix A.

4 RELATED WORKS

Multi-Dataset Training in Neuroscience. Previous work has explored multi-dataset training for extracting latent representations in neuroscience. LFADS (Pandarinath et al., 2018) used session-stitching, but focused on single-animal recordings. Linderman et al. (2019) used hierarchical Bayesian state-space models with switching linear dynamical systems, while Herrero-Vidal et al. (2021) developed a joint model with shared linear dynamics but dataset-specific likelihoods. In contrast to these approaches, we incorporate a more expressive dynamics function that disentangles variabilities across recording sessions. CEBRA (Schneider et al., 2023) and CS-VAE (Yi et al., 2022) extract latent representations but do not learn underlying dynamics. Recently, there has been growing interest in using diverse neural recordings for training large-scale foundation models

²Note that we plot the absolute embedding samples since the likelihood function can introduce arbitrary invariance such as direction flipping, rotation, and so on.

in neuroscience (Ye et al., 2023; Zhang et al., 2023; Caro et al., 2024; Azabou et al., 2024). Our approach shares the same broad goal of pretraining a single model for rapid adaptation on downstream recordings; however, we focus on learning a dynamics model across recordings while these methods leverage transformer-based architectures that encode temporal information indirectly via positional embeddings.

Meta-Learning. Several meta-learning approaches have been developed for few-shot adaptation, including gradient-based methods (Finn et al., 2017; Li et al., 2017; Nichol & Schulman, 2018; Zintgraf et al., 2019). Amongst these, LEO (Rusu et al., 2019) shares the same idea of meta-learning in low-dimensional space of parameter embeddings. However, gradient-based approaches require fine-tuning during test-time, and have had limited success for meta-learning dynamics. Similar to our work (Cotler et al., 2023) also learns an embedding space of dynamics learned from trained RNNs, however, we are interested in learning dynamics directly from data. Some methods for learning generalizable dynamics been previously proposed—DyAD (Wang et al., 2022) adapts across environments by neural style transfer, however it operates on images of dynamical systems, LEADS (Yin et al., 2021) learns a constrained dynamics function that is directly added to some base dynamics function, and CoDA (Kirchmeyer et al., 2022) which learns task-specific parameter changes conditioned on a low-dimensional context similar to our approach. However, these approaches were applied in supervised settings on low-dimensional systems whereas we operate in an unsupervised setting.

5 EXPERIMENTS

We first validate the proposed method on synthetic data and then test our method on neural recordings from the primary motor and premotor cortex. We compare the proposed approach against the following baselines:

Single Session Model. We train a separate model on each dataset. Given sufficient training data, this should result in the best performance, but will fail in trial-limited regimes.

Multi-Session Shared Dynamics. We also consider a model that assumes the same dynamics with dataset-specific likelihoods (Pandarinath et al., 2018; Herrero-Vidal et al., 2021).

Embedding-Input. In this baseline, the embedding is provided as an additional input to the dynamics model. This is a similar formulation to CAVIA (Concat) (Zintgraf et al., 2019) and DYNAMO (Cotler et al., 2023).

Linear Adapter. We additionally test the hypernetwork parametrization proposed in CoDA (Kirchmeyer et al., 2022), where the hypernetwork adapts all parameters as a linear function of the dynamical embedding.

For each experiment, we split each of the M datasets into a training and test set and report reconstruction and forecasting metrics on the test set. To measure the generalization performance, we also report these metrics on held-out datasets. Further details on training and evaluation metrics can be found in Appendix D.

5.1 BIFURCATING SYSTEMS

In these experiments, we test whether our method could capture variations across multiple datasets, particularly in the presence of significant dynamical shifts, such as bifurcations commonly observed in real neural populations. To test this, we chose two parametric classes of dynamical systems: i) a system undergoing a Hopf bifurcation and, ii) the unforced Duffing system. We include the results for training on datasets generated only from the Hopf system in Appendix B.1 and discuss the results of jointly training on both systems here. We briefly outline the data generation process for the Duffing system (with data generation for Hopf included in Appendix B.1).

The latent trajectories for the Duffing system were generated from a family of stochastic differential equations,

$$\dot{z}_1 = z_2 + 5 dW_t, \quad \dot{z}_2 = a^i z_2 - z_1(b^i + cz_1^2) + 5 dW_t \quad (19)$$

with $c = 0.1$, $a, b \in \mathbb{R}$, and dW_t denoting the Wiener process. In Fig. 4A, we visualize how the dynamical system changes as a and b vary. We chose $M = 20$ pairs of (a^i, b^i) values (Fig 11),

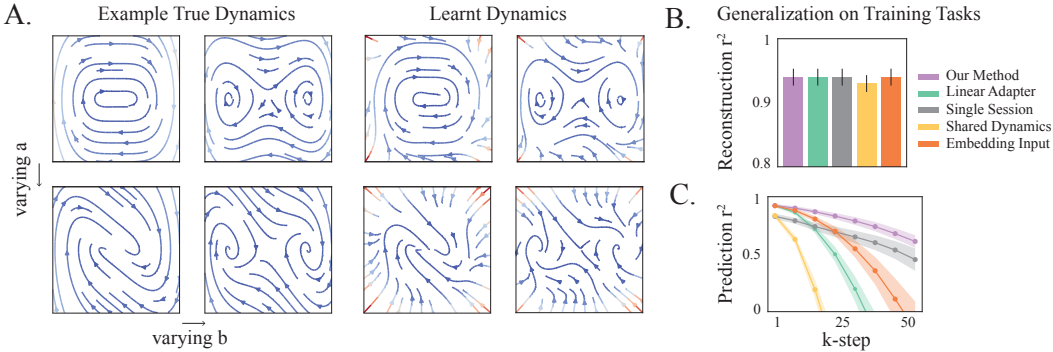


Figure 4: **A.** (Left) True underlying dynamics from some example datasets used for pretraining as a function of parameters a and b and (Right) the embedding conditioned dynamics learnt by our model. **B., C.** Mean reconstruction and forecasting r^2 of the observations for all datasets used for pretraining on test trials.

and generated latent trajectories of length $T = 300$. Observations were generated according to $y_t^i \sim \mathcal{N}(C^i z_t^i, 0.01\mathbb{I})$; the dimensionality of the observations varied between 30 and 100. In addition to these 20 datasets, we included 11 datasets from the Hopf system (Appendix B.2), and used 128 trajectories from each of these 31 datasets for training all methods. We report performance on 64 test trajectories from each dataset. We used $d_e = 2$ for all embedding-conditioned approaches and constrained the hypernetwork to make rank $d^r = 1$ changes for our approach.

Our approach was able to learn a good approximation to the ground-truth dynamics of the Duffing oscillator system while disentangling different dynamical regimes (Fig. 4 A). Apart from learning the underlying topology of dynamics, it also better captured the geometrical properties compared to other embedding-conditioned baselines (Fig. 12). We observed similar results for datasets from the Hopf system—while our approach approximated the ground-truth system well, the Embedding-Input baseline displayed interference between dynamics and the Linear-Adapter learned a poor approximation to the ground-truth system (Fig. 13). Consequently, our approach outperformed other methods on forecasting observations with all methods having comparable reconstruction performance (Fig. 4B, C). Notably, apart from the d^e , we used the same architecture as when training on only the Hopf datasets, and did not observe any drop in performance for our approach, in contrast to baselines (Fig. 10C (Bottom), Fig. 4C).

	$n_s = 1$	$n_s = 8$	$n_s = 16$
Our Method	0.69 ± 0.072	0.78 ± 0.051	0.87 ± 0.037
Linear-Adapter	0.68 ± 0.08	0.79 ± 0.026	0.74 ± 0.039
Single Session	0.47 ± 0.119	0.79 ± 0.014	0.79 ± 0.047
Shared Dynamics	-0.31 ± 0.103	-0.34 ± 0.086	-0.13 ± 0.065
Embedding-Input	0.59 ± 0.084	0.77 ± 0.04	0.74 ± 0.039

Table 1: Few shot forecasting performance ($k = 30$ -step) on 3 held-out datasets as a function of n_s , the number of trials used to learn dataset specific read-in network and likelihood. (± 1 s.e.m)

Next, we tested the few-shot performance of all methods on new datasets, two generated from the Duffing oscillator system and one from the Hopf system, as a function of n_s , the number of trials used for learning the dataset specific read-in network, Ω^i and likelihood. Our approach and the Linear-Adapter demonstrated comparable forecasting performance when using $n_s = 1$ and $n_s = 8$ training trajectories. However, with $n_s = 16$ training trials, unlike other methods, our approach continued to improve and outperformed them (Table 1). This could be explained by looking at the inferred embedding on held-out datasets—as we increased the number of training trajectories, the model was able to consistently align to the “correct” embedding (Fig. 14).

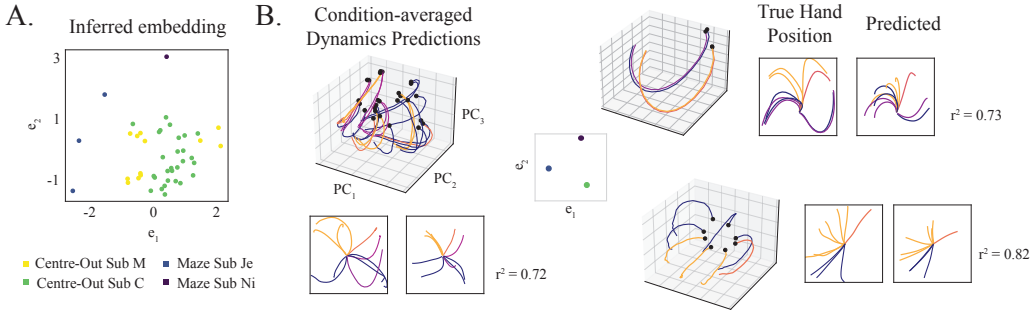


Figure 5: Visualizing the embedding manifold. **A.** Each point corresponds to a sample from the inferred embedding distribution (see eq. 17) corresponding to each recording. **B.** The condition-averaged of latent dynamics projections generated by the model, along with the corresponding real and forecasted behavior.

5.2 MOTOR CORTEX RECORDINGS

We move on to testing the applicability of the proposed approach on neural data. We use single and multi-unit neural population recordings from the motor and premotor cortex during two behavioral tasks—the Centre-Out (CO) and Maze reaching tasks (Perich et al., 2018; Gallego et al., 2020; Churchland et al., 2012). In the CO task, subjects are trained to use a manipulandum to reach one of eight target locations on a screen. In the Maze task, subjects use a touch screen to reach a target location, while potentially avoiding obstacles. These recordings spanned different sessions, animals, and labs, and involved different behavioral modalities, while still having related behavioral components, making them a good testbed for evaluating various methods. For training, we used 40 sessions from the CO task, from subjects M and C, and 4 sessions from the Maze task from subjects Je and Ni. We set the dimensionality of latent dynamics to $d_z = 30$, and used an embedding dimensionality of $d_e = 2$, for all embedding-conditioned dynamics models. For our approach, we constrain the hypernetwork to make rank $d^r = 6$ changes, although we verified that the performance was not sensitive to d^r (Fig 15). As a proxy for how well the various approaches learned the underlying dynamics, we report metrics on inferring the hand velocity using reconstructed and forecasted neural data from the models. Note that we align all recordings to the movement onset (details in Appendix D).

The inferred dynamical embedding displayed distinct structures across behavioral tasks and subjects (Fig. 5A). While the CO task involves more stereotyped straight reaching behavior with the same stimulus conditions across datasets, the Maze task has more complex stimulus statistics which vary across sessions. The family of learned dynamics reflected this heterogeneity across recordings, as visualized by the condition-averaged principal components (PCs) of the latent trajectories generated by the model (Fig. 5B).

Many of the approaches had adequate performance on reconstructing velocity from neural recordings, with our method and Linear Adapter outperforming single session reconstruction performance on the CO task (Fig. 6A, top). However, the single-session models had the best performance on forecasting. Since we are using the same base architecture for all methods, this is expected given enough training data. Notably, our approach managed to balance learning both the CO and Maze tasks relative to other multi-session baselines, with all performing better on the CO task than the Maze (Fig. 6A, bottom). Next, we tested if we can transfer these learned dynamics to new recordings as we varied n_s from 8 to 64 trials for learning the read-in network and likelihood. We used trials from 2 held-out sessions from Sub C and M, as well as 2 sessions from a new subject (Sub T) for evaluating all methods. We observed that our approach consistently performed well on both reconstruction and forecasting for held-out sessions from previously seen subjects, and reached good performance on sessions from Sub T as we increased the training trials (Fig. 6B, C ($n_s = 32$)). Moreover, our method outperformed all other baselines on forecasting, especially in very low-sample regimes, while having comparable reconstruction performance (Fig. 16).

We further investigated the effect of large-scale training for sample-efficient transfer on downstream tasks by only pretraining the model on 128 trials from 4 sessions spanning different tasks and subjects.

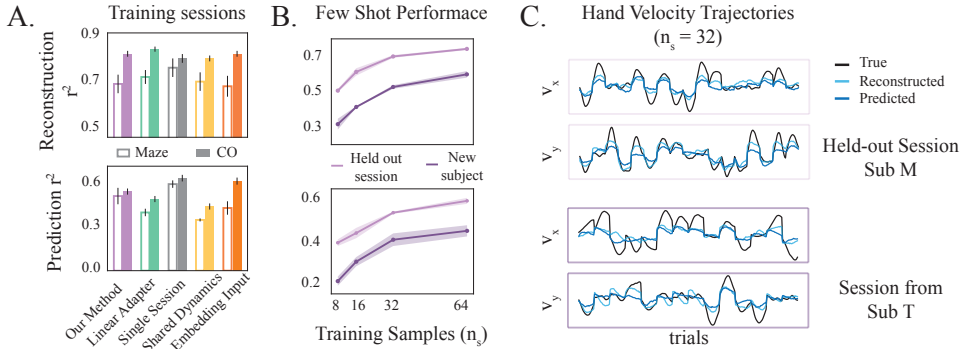


Figure 6: **A.** (top) r^2 for hand velocity decoding from reconstructed and (bottom) forecasted neural observations for Maze and Centre-Out sessions. **B.** Behavior reconstruction (top) and forecasting (bottom) performance on held-out sessions and sessions from a new subject as a function of the number of training samples. **C.** Hand velocity trajectories (400 ms after movement onset) predicted by our approach on 17 test trials from held-out session (top) and 13 test trials from a session on a new subject (bottom), after using $n_s = 32$ trials for aligning to the pre-trained model.

Even in this case, the embedding distribution displayed clear clustering based on the task and subject. Moreover, the model performed comparably to the Single-Session model on reconstruction, while outperforming it on prediction for both tasks (Fig. 17 A, B). However, it demonstrated poor performance on new sessions given limited trials for learning the read-in and likelihood parameters (Fig. 17 C), underscoring the importance of large-scale training for generalizing to novel settings.

Finally, we probed the differences in the latent state evolution given the same initial condition while interpolating across the learned embedding. In order to do this, we chose an example session from the Maze and CO datasets and obtained their corresponding dynamical embedding from the model, shown as a solid blue and green circle in Fig. 7 (middle), respectively. A grid of points was sampled around each of these inferred embeddings (shown as shaded squares in Fig. 7 middle), and for each point we obtained the corresponding low-rank parameter changes to generate the latent trajectories. We observed that the embedding space learned a continuous representation of dynamics, which was reflected in similar predicted behaviors close to the original learned embedding (Fig 7). Interestingly, when we interpolated through the entire embedding space, the predicted behavior and corresponding dynamics continuously varied as well. Specifically, the predicted behavior and dynamics trajectories on the CO session demonstrated similarities over a large portion of the embedding space, with the trajectories shifting to more curved reaches further from the original embedding (Fig. 18). On the Maze task, the trajectories demonstrated more heterogeneity in responses, and decayed to a fixed point further away from the original embedding (Fig. 19).

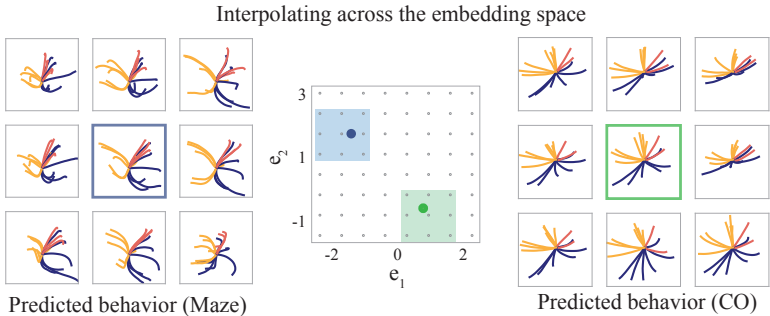


Figure 7: The predicted behavior for a Maze (Sub Je) session and CO (Sub C) session at 9 grid points around the original inferred embedding. The point closest to the original embedding is highlighted in blue and green respectively.

6 DISCUSSION

We present a novel framework for jointly inferring and learning latent dynamics from heterogeneous neural recordings across sessions/subjects during related behavioral tasks. To the best of our knowledge, this is the first approach that facilitates learning a family of dynamical systems from heterogeneous recordings in a unified latent space, while providing a concise, interpretable manifold over dynamical systems. Our meta-learning approach mitigates the challenges of statistical inference from limited data, a common issue arising from the high flexibility of models used to approximate latent dynamics. Empirical evaluations demonstrate that the learned embedding manifold provides a useful inductive bias for learning from limited samples, with our proposed parametrization offering greater flexibility in capturing diverse dynamics while minimizing interference. We observe that the generalization of our model depends on the amount of training data—when trained on smaller datasets, the model learns specialized solutions, whereas more data allows it to learn shared dynamical structures. This work enhances our capability to integrate, analyze, and interpret complex neural dynamics across diverse experimental conditions, broadening the scope of scientific inquiries possible in neuroscience.

LIMITATIONS AND FUTURE WORK

Our current framework uses event aligned neural observations; in the future, it would be useful to incorporate task-related events, to broaden its applicability to complex, unstructured tasks. Further, the model’s generalization to novel settings depends on accurate embedding inference, a challenge noted in previous works that disentangle task inference and representation learning (Hummos et al., 2024). While our latent dynamics parametrization is expressive, it assumes shared structure across related tasks. Future work could extend the model to accommodate recordings without expected shared structures (for instance, by adding modularity (Márton et al., 2021)). Investigating the performance of embedding-conditioned low-rank adaptation on RNN-based architectures presents another avenue for future research. Finally, the embedding manifold provides a map for interpolating across different dynamics. While we focus on rapid learning in this paper, our framework could have interesting applications for studying inter-subject variability, learning-induced changes in dynamics, or changes in dynamics across tasks in the future.

REFERENCES

- Mehdi Azabou, Vinam Arora, Venkataramana Ganesh, Ximeng Mao, Santosh Nachimuthu, Michael Mendelson, Blake Richards, Matthew Perich, Guillaume Lajoie, and Eva Dyer. A unified, scalable framework for neural population decoding. *Advances in Neural Information Processing Systems*, 36, 2024.
- Samuel R Bowman, Luke Vilnis, Oriol Vinyals, Andrew M Dai, Rafal Jozefowicz, and Samy Bengio. Generating sentences from a continuous space. *arXiv preprint arXiv:1511.06349*, 2015.
- Josue Ortega Caro, Antonio H. de O. Fonseca, Christopher Averill, Syed A. Rizvi, Matteo Rosati, James L. Cross, Prateek Mittal, Emanuele Zappala, Daniel Levine, Rahul M. Dhodapkar, Insu Han, Amin Karbasi, Chadi G. Abdallah, and David van Dijk. Brainlm: A foundation model for brain activity recordings. *bioRxiv*, 2024.
- Mark M Churchland, John P Cunningham, Matthew T Kaufman, Justin D Foster, Paul Nuyujukian, Stephen I Ryu, and Krishna V Shenoy. Neural population dynamics during reaching. *Nature*, 487(7405):51–56, 2012.
- Jordan Cotler, Kai Sheng Tai, Felipe Hernández, Blake Elias, and David Sussillo. Analyzing populations of neural networks via dynamical model embedding. *arXiv [cs.LG]*, February 2023.
- Matthew Dowling, Yuan Zhao, and Il Memming Park. eXponential FAmily dynamical systems (XFADS): Large-scale nonlinear gaussian state-space modeling. In *Advances in Neural Information Processing Systems (NeurIPS)*, December 2024.
- Laura N. Driscoll, Lea Duncker, and Christopher D. Harvey. Representational drift: Emerging theories for continual learning and experimental future directions. *Current Opinion in Neurobiology*, 76: 102609, 2022.

- Laura N. Driscoll, Krishna Shenoy, and David Sussillo. Flexible multitask computation in recurrent networks utilizes shared dynamical motifs. *Nature Neuroscience*, 27(7):1349–1363, 2024.
- Chelsea Finn, Pieter Abbeel, and Sergey Levine. Model-agnostic meta-learning for fast adaptation of deep networks. In *International conference on machine learning*, pp. 1126–1135. PMLR, 2017.
- Tomer Galanti and Lior Wolf. On the modularity of hypernetworks. *Advances in Neural Information Processing Systems*, 33:10409–10419, 2020.
- Juan A. Gallego, Matthew G. Perich, Stephanie N. Naufel, Christian Ethier, Sara A. Solla, and Lee E. Miller. Cortical population activity within a preserved neural manifold underlies multiple motor behaviors. *Nature Communications*, 9(1):4233, 2018.
- Juan A Gallego, Matthew G Perich, Raeed H Chowdhury, Sara A Solla, and Lee E Miller. Long-term stability of cortical population dynamics underlying consistent behavior. *Nature neuroscience*, 23(2):260–270, 2020.
- David Ha, Andrew M Dai, and Quoc V Le. Hypernetworks. In *International Conference on Learning Representations*, 2016.
- Pedro Herrero-Vidal, Dmitry Rinberg, and Cristina Savin. Across-animal odor decoding by probabilistic manifold alignment. *Advances in Neural Information Processing Systems*, 34:20360–20372, 2021.
- Ali Hummos, Felipe del Río, Brabeeba Mien Wang, Julio Hurtado, Cristian B. Calderon, and Guangyu Robert Yang. Gradient-based inference of abstract task representations for generalization in neural networks, 2024.
- Matthieu Kirchmeyer, Yuan Yin, Jérémie Donà, Nicolas Baskiotis, Alain Rakotomamonjy, and Patrick Gallinari. Generalizing to new physical systems via context-informed dynamics model. In *International Conference on Machine Learning*, pp. 11283–11301. PMLR, 2022.
- Rahul G Krishnan, Uri Shalit, and David Sontag. Deep kalman filters. *arXiv preprint arXiv:1511.05121*, 2015.
- Zhenguo Li, Fengwei Zhou, Fei Chen, and Hang Li. Meta-sgd: Learning to learn quickly for few-shot learning. *arXiv preprint arXiv:1707.09835*, 2017.
- Scott Linderman, Annika Nichols, David Blei, Manuel Zimmer, and Liam Paninski. Hierarchical recurrent state space models reveal discrete and continuous dynamics of neural activity in c. elegans. *BioRxiv*, pp. 621540, 2019.
- Thomas Zhihao Luo, Timothy Doyeon Kim, Diksha Gupta, Adrian G Bondy, Charles D Kopec, Verity A Elliot, Brian DePasquale, and Carlos D Brody. Transitions in dynamical regime and neural mode underlie perceptual decision-making. *bioRxiv*, pp. 2023–10, 2023.
- Niru Maheswaranathan, Alex Williams, Matthew Golub, Surya Ganguli, and David Sussillo. Universality and individuality in neural dynamics across large populations of recurrent networks. In H. Wallach, H. Larochelle, A. Beygelzimer, F. d'Alché-Buc, E. Fox, and R. Garnett (eds.), *Advances in Neural Information Processing Systems*, volume 32. Curran Associates, Inc., 2019.
- Christian David Márton, Léo Gagnon, Guillaume Lajoie, and Kanaka Rajan. Efficient and robust multi-task learning in the brain with modular latent primitives. *arXiv preprint arXiv:2105.14108*, 2021.
- Aditya Nair, Tomomi Karigo, Bin Yang, Surya Ganguli, Mark J. Schnitzer, Scott W. Linderman, David J. Anderson, and Ann Kennedy. An approximate line attractor in the hypothalamus encodes an aggressive state. *Cell*, 186(1):178–193.e15, 2023.
- Alex Nichol and John Schulman. Reptile: a scalable metalearning algorithm. *arXiv preprint arXiv:1803.02999*, 2(3):4, 2018.

- Chethan Pandarinath, Daniel J. O’Shea, Jasmine Collins, Rafal Jozefowicz, Sergey D. Stavisky, Jonathan C. Kao, Eric M. Trautmann, Matthew T. Kaufman, Stephen I. Ryu, Leigh R. Hochberg, Jaimie M. Henderson, Krishna V. Shenoy, L. F. Abbott, and David Sussillo. Inferring single-trial neural population dynamics using sequential auto-encoders. *Nature Methods*, 15(10):805–815, 2018.
- Matthew G Perich, Juan A Gallego, and Lee E Miller. A neural population mechanism for rapid learning. *Neuron*, 100(4):964–976, 2018.
- Andrei A. Rusu, Dushyant Rao, Jakub Sygnowski, Oriol Vinyals, Razvan Pascanu, Simon Osindero, and Raia Hadsell. Meta-learning with latent embedding optimization, 2019.
- Mostafa Safaie, Joanna C. Chang, Junchol Park, Lee E. Miller, Joshua T. Dudman, Matthew G. Perich, and Juan A. Gallego. Preserved neural dynamics across animals performing similar behaviour. *Nature*, 623(7988):765–771, 2023.
- Marine Schimel, Ta-Chu Kao, Kristopher T Jensen, and Guillaume Hennequin. iLQR-VAE : control-based learning of input-driven dynamics with applications to neural data. In *International Conference on Learning Representations*, 2022.
- Steffen Schneider, Jin Hwa Lee, and Mackenzie Weygandt Mathis. Learnable latent embeddings for joint behavioural and neural analysis. *Nature*, 617(7960):360–368, 2023.
- Elia Turner and Omri Barak. The simplicity bias in multi-task rnns: Shared attractors, reuse of dynamics, and geometric representation. In A. Oh, T. Naumann, A. Globerson, K. Saenko, M. Hardt, and S. Levine (eds.), *Advances in Neural Information Processing Systems*, volume 36, pp. 25495–25507. Curran Associates, Inc., 2023.
- Rui Wang, Robin Walters, and Rose Yu. Meta-learning dynamics forecasting using task inference. *Advances in Neural Information Processing Systems*, 35:21640–21653, 2022.
- Joel Ye, Jennifer L. Collinger, Leila Wehbe, and Robert Gaunt. Neural data transformer 2: Multi-context pretraining for neural spiking activity. *bioRxiv*, 2023.
- Daiyao Yi, Simon Musall, Anne Churchland, Nancy Padilla-Coreano, and Shreya Saxena. Disentangled multi-subject and social behavioral representations through a constrained subspace variational autoencoder (cs-vae). *bioRxiv*, pp. 2022–09, 2022.
- Yuan Yin, Ibrahim Ayed, Emmanuel de Bézenac, Nicolas Baskiotis, and Patrick Gallinari. Leads: Learning dynamical systems that generalize across environments. *Advances in Neural Information Processing Systems*, 34:7561–7573, 2021.
- Daoze Zhang, Zhizhang Yuan, YANG YANG, Junru Chen, Jingjing Wang, and Yafeng Li. Brant: Foundation model for intracranial neural signal. In A. Oh, T. Naumann, A. Globerson, K. Saenko, M. Hardt, and S. Levine (eds.), *Advances in Neural Information Processing Systems*, volume 36, pp. 26304–26321. Curran Associates, Inc., 2023.
- Luisa Zintgraf, Kyriacos Shiarli, Vitaly Kurin, Katja Hofmann, and Shimon Whiteson. Fast context adaptation via meta-learning. In *International Conference on Machine Learning*, pp. 7693–7702. PMLR, 2019.

A DETAILS OF MOTIVATING EXPERIMENT FROM SECTIONS 2 AND 3.3

Data Generation. The latent dynamics follow a two-dimensional limit cycle which is defined by the following system of equations

$$\begin{aligned} \dot{r} &= r(1-r)^2, \\ \dot{\theta} &= \omega^i, \\ z_1^i &= r \cos \theta + 5 dW_t, \quad z_2^i = r \sin \theta + 5 dW_t, \end{aligned}$$

where $\omega^i, i \in \{1, \dots, M\}$ is the dataset specific velocity and dW_t is the Wiener process. Specifically, for the experiment with $M = 2$ datasets, we set $\omega^1 = 2$ and $\omega^2 = 5$; for the experiment with $M = 20$ datasets, we uniformly sampled 20 values for ω^i between 0.25 and 5. For each value of ω^i , we generated 128 latent trajectories for training, 64 for validation and 64 for testing, each of length $T = 300$, where we used Euler-Mayurama with Δt of 0.04 for integration. Observations were generated according to $y_t^i \sim \mathcal{N}(C^i z_t^i, R)$ where $R = 0.01 * I$ and the elements of the readout matrix C^i were sampled from $\mathcal{N}(0, I/\sqrt{d^z})$; the dimensionality of the observations varied between 30 and 100.

1-shot Performance. We evaluated the generalization performance of our approach on a new dataset with $\omega^{M+1} = 4.1$, which was not included in the training set, by using 1 training trajectory to train a new read-in network, Ω^{M+1} and likelihood p_ϕ^{M+1} . After training, the model displayed similar prediction performance on the new dataset ($r_{k=50}^2 = 0.94 \pm 0.001$) (Fig. 8).

No Model Mismatch.

Here, we investigated the performance of our approach when there is no mismatch between the proposed generative model and the true system. For this experiment, we generated synthetic data from the model trained on $M = 20$ datasets. We used the observations from validation trials till $t = 100$ to infer the embedding, e^i , and latent state, z_t^i . We subsequently used the dynamics model to generate latent trajectories of length 250, $z_{t+1:t+250}^i$ and mapped them back to the observations via the learned likelihood function. We re-trained a model with the same architecture while keeping the likelihood readout and read-in parameters fixed since the likelihood could arbitrarily flip the direction of the flow field.

Similar to the ground truth generative model, the inferred embedding co-varied with the different velocities (Fig. 9A, left). Further, the model recovered the correct topology of the ground truth dynamics (Fig. 9B), reflected in the forecasting performance on held out test trials (Fig. 9A, right).

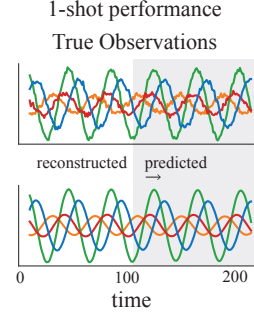


Figure 8: (Top) True observations on new data with $\omega = 4.1$ and (Bottom) the corresponding reconstructed and predicted observations after aligning to the trained model.

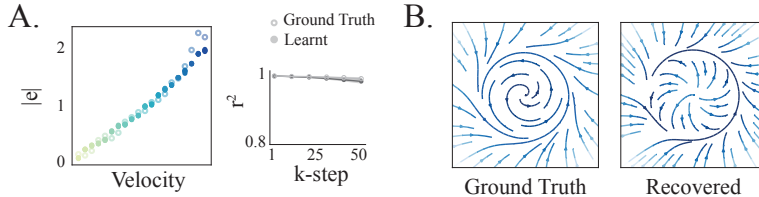


Figure 9: **A.** (Left) Samples from the inferred embedding (see eq. 17) after training on trajectories generated from our model overlaid on the ground truth embeddings. (Right) Forecasting performance of the trained and ground truth model on held out trials. **B.** Ground truth dynamics generated from an embedding sample and the corresponding recovered dynamics.

B SYNTHETIC BIFURCATING SYSTEMS

B.1 HOPF BIFURCATION

Data Generation. Latent trajectories were generated from the following two-dimensional dynamical system,

$$\dot{z}_1 = z_2 + 5 dW_t, \quad \dot{z}_2 = -z_1 + (\mu^i - z_1^2)z_2 + 5 dW_t, \quad (20)$$

where the parameter μ^i controls the topology of the dynamics. Specifically, when $\mu^i < 0$, this system follows fixed point dynamics, and when $\mu > 0$ the system bifurcates to a limit cycle.

We uniformly sampled $M = 21$ values of μ^i between -1.5 and 1.5, and for each μ^i , we generated 128 trajectories for training and 64 for testing, each trajectory was $T = 350$. Observations were generated

according to $y_t^i \sim \mathcal{N}(C^i z_t^i, R)$ where $R = 0.01 * I$ and the elements of the readout matrix C^i were sampled from $\mathcal{N}(0, I/\sqrt{d^z})$; the dimensionality of the observations varied between 30 and 100. For evaluating few-shot performance, we generated two additional novel datasets where $\mu^{M+1} = -0.675$ and $\mu^{M+2} = 1.125$ (both values were not included in the training set).

Results. For all embedding conditioned approaches, we set $d_e = 1$ and learned a rank-1 change to the dynamics for our approach. Our approach successfully learned both dynamical regimes present in the datasets and the embedding distribution encoded differences in these dynamics with high certainty given limited time bins on test trials(Fig. 10A, B). While all approaches performed well on reconstructing observations on these datasets, our approach and the Embedding-Input outperformed other multi-session baselines on forecasting (Fig 10C). We also evaluated the generalization performance of all methods on the 2 held-out datasets as a function of training data used for training the read-in network and observed similar trends as demonstrated by the reconstruction and k-step = 20 r^2 on test trials from these datasets, shown in Table 2.

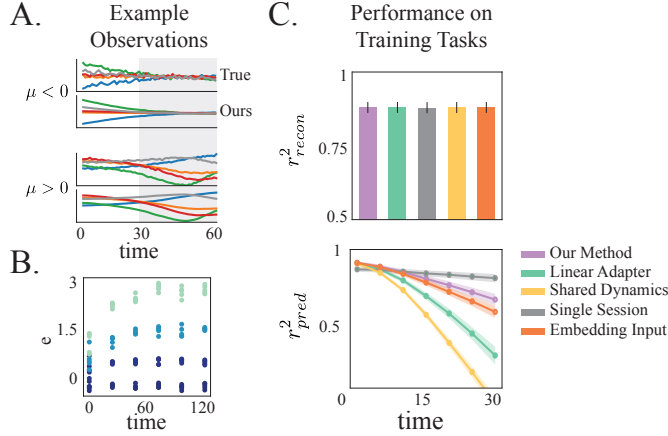


Figure 10: **A.** Example observations along with the reconstructed and predicted observations from our approach for the fixed point (Top) and limit cycle (Bottom) dynamical regimes. **B.** Samples from the embedding as a function of the number of time bins in the test trials for 4 example datasets. **C.** Reconstruction (Top) and forecasting (Bottom) performance of all approaches on the datasets used for pretraining.

	Reconstruction		Forecasting	
	$n_s = 1$	$n_s = 8$	$n_s = 1$	$n_s = 8$
Ours	0.85 ± 0.054	0.89 ± 0.04	0.64 ± 0.1	0.69 ± 0.07
Linear-Adapter	0.84 ± 0.059	0.89 ± 0.04	-0.1 ± 0.34	0.55 ± 0.08
Single Session	0.8 ± 0.054	0.88 ± 0.044	0.27 ± 0.08	0.77 ± 0.03
Shared Dynamics	0.83 ± 0.068	0.89 ± 0.04	0.32 ± 0.08	0.32 ± 0.04
Embedding-Input	0.86 ± 0.049	0.89 ± 0.04	0.61 ± 0.09	0.56 ± 0.11

Table 2: Few-shot reconstruction and forecasting performance (k-step=20) for held-out datasets in B.1 where n_s is the number of trials used for learning the dataset specific read-in network and likelihood.

B.2 DUFFING SYSTEM

Data Generation. For the Duffing system described in 19, we set $c = \frac{1}{10}$ and varied values of a and b (shown in blue, Fig. 11) for generating 20 datasets. We additionally used 11 datasets from B.1 obtained by uniformly sampling μ between -1.5 and 1.5. For few shot evaluation of various approaches, we used two held-out datasets from the Duffing system (shown in orange, Fig. 11), as well as a dataset from the Hopf example generating by setting $\mu = -1.8$.

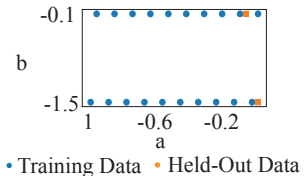


Figure 11: (a^i, b^i) values used to generate different datasets from the Duffing system.

All empirical evaluation was performed on 64 test trials from each dataset.

C ADDITIONAL FIGURES

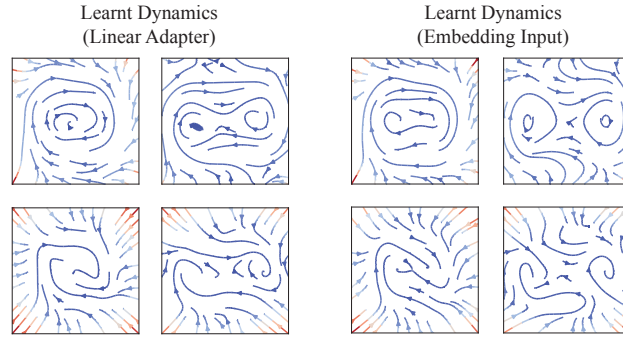


Figure 12: (Left) Dynamics learnt by Linear-Adapter and (Right) Embedding-Input corresponding to the example dynamics on the true system shown in Fig. 4A.

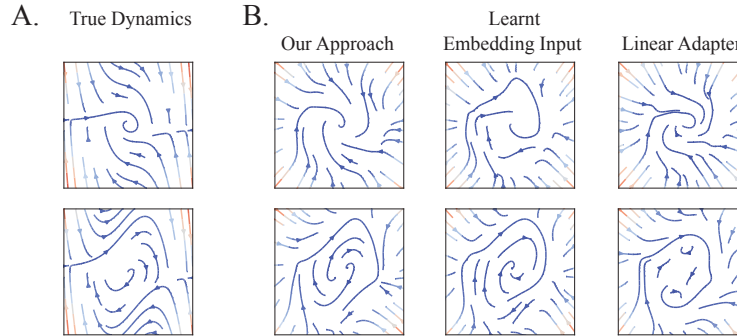


Figure 13: (Left) True dynamics from example datasets used for pretraining in experiment 5.1. (Right) Dynamics Learnt by different embedding-conditioned parametrizations.

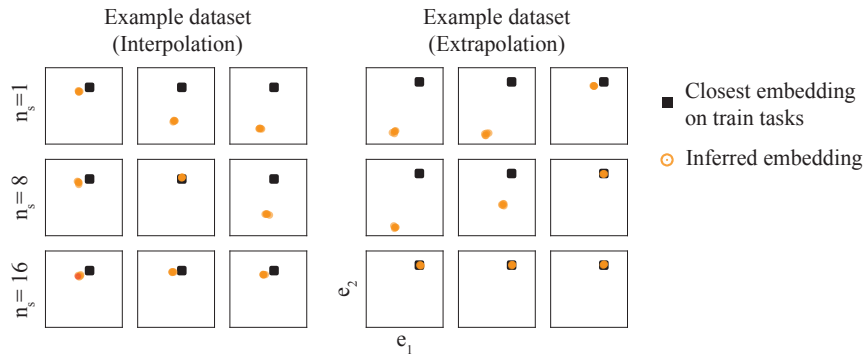


Figure 14: Samples from the embedding distribution as a function of the number of training trajectories on 3 seeds on held-out datasets from the Duffing system (denoted by orange, Fig. 11)

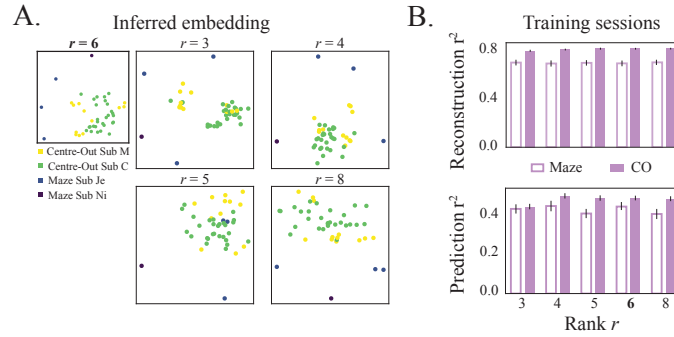


Figure 15: **A.** Sample from the inferred embedding for different ranks (best of 3 seeds). **B.** The behavior reconstruction (Top) and prediction (Bottom) r^2 for different ranks averaged over 3 training seeds.

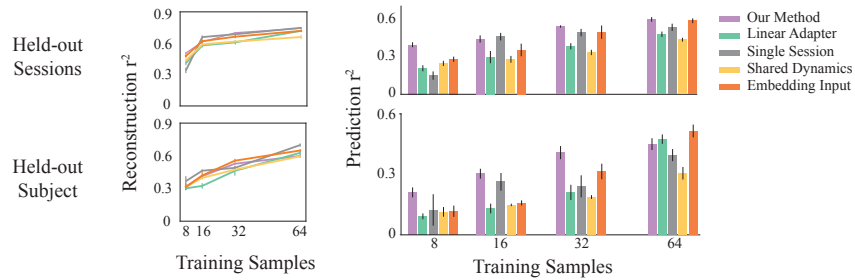


Figure 16: Behavior reconstruction (Left) and forecasting (Right) for all methods as a function of the number of training samples for held-out sessions from Sub M and C, and two sessions from a held-out Subject.

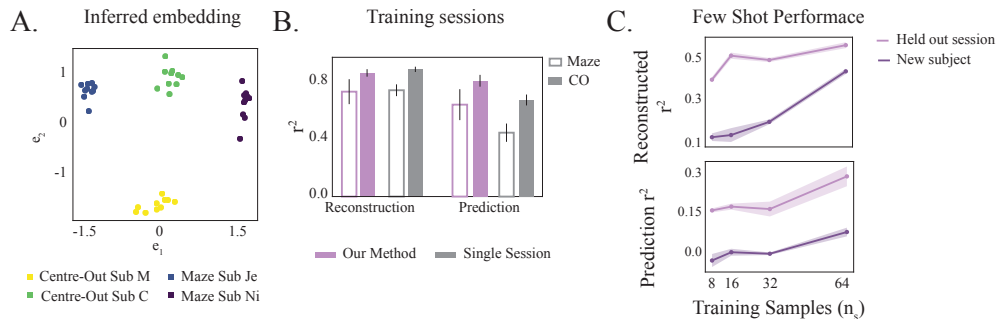


Figure 17: **A.** Samples from the embedding distribution after training our approach using 2 CO sessions from Sub C and M, and 2 Maze sessions from Sub Je and Ni. **B.** Reconstruction and forecasting performance of the model on held out test trials relative to the Single Session models. **C.** Few-shot reconstruction and forecasting performance on held out sessions and a new subject (Sub T).

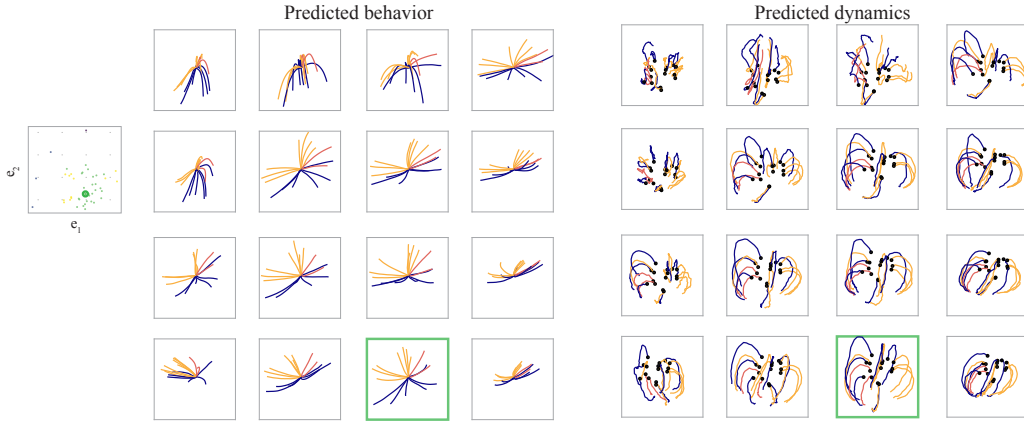


Figure 18: (Left) Grid points used for generating the latent trajectories and behavior prediction with the embedding distribution overlaid. The true embedding of the CO session from Sub C used to inferring the initial condition is highlighted in green. (Right) Single trials of the predicted hand position and PCs of latent dynamics trajectories.

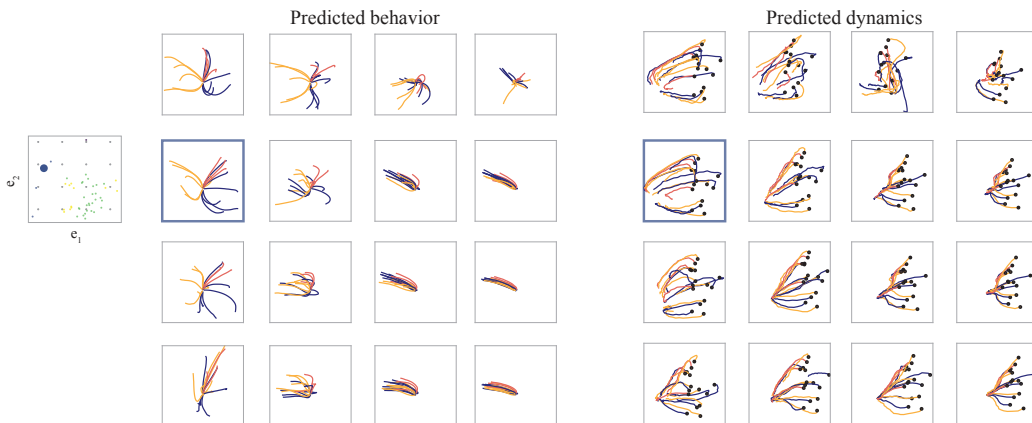


Figure 19: Same as 18 but for a Maze session from Sub Je (highlighted in blue).

D EXPERIMENT DETAILS

D.1 TRAINING

Since CAVIA (Concat) (Zintgraf et al., 2019), DYNAMO (Cotler et al., 2023) and CoDA (Kirchmeyer et al., 2022) have not been developed for joint inference and learning of dynamics, we use our framework for inference with modifications to the parametrization of the embedding conditioned dynamics function on all experiments. For our method and CoDA, we restricted parameter changes to the input, \mathbf{W}_{in} , and hidden weights, \mathbf{W}_{hh} . We additionally included the Frobenius norm on the embedding-conditioned weight change $\|h_\varphi(e^i)\|_F$ along with the ELBO (eq. 15) for both approaches.

Synthetic Experiments. For the results reported in B.1 and 5.1, we used the Adam optimizer with weight decay and a Cosine annealing schedule on the learning rate for pretraining all approaches.

Motor Cortex Recordings. We binned the spiking activity in 20ms bins and smoothed it with a 25ms Gaussian filter to obtain the rates for all datasets. We further removed neurons that had a firing rate of less than 0.1Hz and aligned the neural activity to movement onset. We used 512 trials when available or 80 percent of the trials, each of length 36, for training all methods.

We used the LAMB optimizer for pretraining all multi-session methods on the motor cortex recordings and used Adam with weight decay for the single-session models, with a Cosine annealing schedule on the learning rate in both cases. We also incorporated masking during training for all approaches to encourage learning better latent dynamics. Specifically, we sampled the latent state from the dynamics instead of the state inference network on randomly masked time bins to compute the likelihood.

Aligning New Data. We pretrained all multi-session approaches for 3 seeds and picked the best performing model to evaluate few-shot performance. When aligning new data to this pre-trained model, we trained the dataset-specific read-in network, Ω^i and likelihood functions p_ϕ^i for the new dataset, in addition to the state noise, Q^i , by optimizing the ELBO for new data (eq. 15). We used Adam with weight decay for aligning, and additionally incorporated masking when aligning held-out motor cortex datasets.

D.2 METRICS

Synthetic Experiments. We report the r^2 on observation reconstruction for test trials over the entire length of the trial for all approaches. In order to evaluate the forecasting performance, we use observations till time t and sample the corresponding latent trajectories, $z_{0:t}^i$, from the inference network and the corresponding e^i for the embedding-conditioned methods. We subsequently use the learned dynamics model to generate K steps ahead from $z_{t+1:t+K}^i$ and map these generated trajectories back to the observations. The k -step r^2 for each dataset is computed as,

$$r_k^2 = 1 - \frac{\sum_{i=1}^M (y_k - \hat{y}_k)^2}{\sum_{i=1}^M (y_k - \bar{y})^2}$$

where \bar{y} is the mean activity during the trial, and M is the number of test trials.

Motor Cortex Recordings. On the motor cortex experiments, we report behavior decoding from the reconstructed and forecasted observations for all methods. Specifically, for each session, we trained a linear behavior decoder from the neural observations to the hand velocity of the subject, assuming a uniform delay of 100ms between neural activity and behavior for all sessions.

After training all methods, we use reconstructed observations from the test trials to evaluate the behavior reconstruction r^2 . For evaluating the decoding performance from forecasted observations, we used the first 13 time bins (around time till movement onset) to estimate the latent state and embedding, and subsequently use the trained dynamics model to forecast the next 20 time bins. The observations corresponding to these forecasted trajectories were used to evaluate the prediction r^2 .

D.3 HYPERPARAMETERS

Synthetic Examples. We used the following architecture for pretraining all methods, with $d^e = 1$ for the Motivating example and Hopf bifurcating system, and $d^e = 2$ for the combined Duffing and Hopf example.

- Inference network
 - Ω^i : MLP(d^{y^i} , 64, 8)
 - q_α : [GRU(16), Linear(16, $2 \times d^e$)]
 - q_β : [biGRU(64), Linear(128, 4)]
- Generative model
 - f_θ : MLP(2, 32, 32, 2)
 - h_ϑ : MLP(d^e , 16, 16, $(64 + 33) \times d^r$)
 - p_{ϕ^i} : [Linear(2, d^{y^i})]
- Training
 - lr: 0.005
 - weight decay: 0.001
 - batch size: 8 from each dataset

Motor Cortex Experiment.

- Inference network
 - Ω^i : MLP(d^{y^i} , 128, Dropout(0.6), 64)
 - q_α : [GRU(64), Linear(64, $2 \times d^e$)]
 - q_β : [biGRU(128), Linear(128, 60)]
- Generative model
 - f_θ : MLP(30, 128, 128, 30)
 - h_ϑ : MLP(d^e , 64, 64, $(256 + 158) \times d^r$)
 - p_{ϕ^i} : [Linear(30, d^{y^i})]
- Training
 - lr: 0.01
 - weight decay: 0.05
 - batch size: 64 trials from 20 datasets